International Journal of Hydrogen Energy 54 (2024) 1307–1318

Contents lists available at ScienceDirect

International Journal of Hydrogen Energy

journal homepage: www.elsevier.com/locate/he

Enhanced microalgal hydrogen production subsisting on visible light TiO_2 nanotubes photocatalyst pre-treated palm kernel expeller

Nurul Tasnim Sahrin [a], Fatima Musa Ardo [a], Uganeeswary Suparmaniam [b], Anita Ramli [a], Jin Chung Sin [c,d], Sze Mun Lam [d,e], Wen Da Oh [f], Boredi Silas Chidi [g], Hui-Suan Ng [h,i], Muhammad Kashif Shahid [j], Ahmed M. Tawfeek [k], Kuan Shiong Khoo [l,m,**], Jun Wei Lim [a,n,*]

[a] HICoE-Centre for Biofuel and Biochemical Research, Institute of Self-Sustainable Building, Department of Fundamental and Applied Sciences, Universiti Teknologi PETRONAS, 32610, Seri Iskandar, Perak Darul Ridzuan, Malaysia
[b] HICoE-Centre for Biofuel and Biochemical Research, Institute of Self-Sustainable Building, Department of Chemical Engineering, Universiti Teknologi PETRONAS, 32610, Seri Iskandar, Perak Darul Ridzuan, Malaysia
[c] Department of Petrochemical Engineering, Faculty of Engineering and Green Technology, Universiti Tunku Abdul Rahman, Jalan Universiti, Bandar Barat, 31900, Kampar, Perak, Malaysia
[d] College of Environmental Science and Engineering, Guilin University of Technology, Guilin, 541004, China
[e] Department of Environmental Engineering, Faculty of Engineering and Green Technology, Universiti Tunku Abdul Rahman, Jalan Universiti, Bandar Barat, 31900, Kampar, Perak, Malaysia
[f] School of Chemical Sciences, Universiti Sains Malaysia, 11800, Penang, Malaysia
[g] Bioresource Engineering Research Group (BioERG), Department of Biotechnology and Consumer Science, Faculty of Applied Sciences, Cape Peninsula University of Technology, Corner of Hanover, and Tennant Street, Zonnebloem, Cape Town, 8000, South Africa
[h] Faculty of Engineering, Technology and Built Environment, UCSI University, UCSI Heights, 56000, Cheras, Kuala Lumpur, Malaysia
[i] UCSI-Cheras Low Carbon Innovation Hub Research Consortium, UCSI University, 56000, Cheras, Kuala Lumpur, Malaysia
[j] Research Institute of Environment & Biosystem, Chungnam National University, Yuseonggu, Daejeon, 34134, Republic of Korea
[k] Department of Chemistry, College of Science, King Saud University, Riyadh, 11451, Saudi Arabia
[l] Department of Chemical Engineering and Materials Science, Yuan Ze University, Taoyuan, Taiwan
[m] Centre for Herbal Pharmacology and Environmental Sustainability, Chettinad Hospital and Research Institute, Chettinad Academy of Research and Education, Kelambakkam, 603103, Tamil Nadu, India
[n] Department of Biotechnology, Saveetha School of Engineering, Saveetha Institute of Medical and Technical Sciences, Chennai, 602105, India

ARTICLE INFO

Handling Editor: Ibrahim Dincer

Keywords:
TiO_2 nanotubes
Photocatalyst
Microalgae
Green hydrogen production
Fermentation
Palm kernel expeller

ABSTRACT

The present study investigated the application of photocatalytic process using TiO_2 nanotubes (NTs) photocatalyst as an effective pre-treatment method for palm kernel expeller (PKE) in increasing its biodegradability to enhance the microalgal hydrogen production via dark fermentation. A series of TiO_2 NTs photocatalysts were synthesized via employing electrochemical anodization of Ti foil at various voltages each in different types of electrolytes (choline chloride-ethylene glycol (ChCl-EG), choline chloride-urea (ChCl-U), choline chloride-glycerol (ChCl-Gly)). Increasing trend of average NTs diameters at 26.14 ± 1.30, 73.01 ± 1.94 and 122.00 ± 13.32 nm was observed for 25, 30 and 35 V in synthesizing TiO_2 NTs using suitable ChCl-EG electrolyte, respectively. The high 35 V had resulted in noticeable pore ruptures within this TiO_2 NTs photocatalyst. The PKE pre-treated by TiO_2 NTs photocatalyst anodized at optimum 30 V in ChCl-EG electrolyte had demonstrated the highest releases of biochemical oxygen demand (BOD_5) and soluble chemical oxygen demand (SCOD) concentrations at 594 and 607 mg/L, respectively. Moreover, the microalgal efficiency of BOD_5 conversion and hydrogen yield were also consistently maintained from third cycle of TiO_2 NTs photocatalyst's reutilizations, signifying the stability of TiO_2 NTs photocatalyst.

* Corresponding author. HICoE-Centre for Biofuel and Biochemical Research, Institute of Self-Sustainable Building, Department of Fundamental and Applied Sciences, Universiti Teknologi PETRONAS, 32610 Seri Iskandar, Perak Darul Ridzuan, Malaysia.
** Corresponding author. Department of Chemical Engineering and Materials Science, Yuan Ze University, Taoyuan, Taiwan.
E-mail addresses: kuanshiong.khoo@saturn.yzu.edu.tw (K.S. Khoo), junwei.lim@utp.edu.my, jun_wei_85@yahoo.com (J.W. Lim).

https://doi.org/10.1016/j.ijhydene.2023.12.099
Received 30 August 2023; Received in revised form 2 December 2023; Accepted 10 December 2023
Available online 20 December 2023

1. Introduction

The obligatory task of developing sustainable energy sources has become increasingly imperative in the near future due to the extensive impacts of global warming and the escalating challenges surrounding the energy supplies worldwide. Presently, the atmospheric carbon dioxide concentration has reached a historical high of 420 ppm [1,2]. In this context, hydrogen, as a clean-burning fuel, holds promise to serve as a zero-carbon substitute for fossil fuels [3]. Accordingly, the hydrogen molecules can be generated through various chemical processes such as hydrocarbon reforming using natural sources like natural gas, as well as non-reforming methods, e.g., gasification and water splitting [4]. However, the focus on biofuel research and development has notably shifted towards the innovative and efficient biomass-based feedstock, aiming to produce green hydrogen as the final product [5,6].

Microalgae offer several advantages as a feedstock for green hydrogen production. These photosynthetic microorganisms possess the remarkable capability to sequester both environmental and anthropogenic carbon dioxide, while releasing oxygen molecules into the environment, making them strategically significant in addressing the global warming issues [7,8]. Previous studies had confirmed the high carbohydrate contents of various microalgal species, making them a viable option for biofuel production [9,10]. However, it is crucial to consider the choice of organic carbon sources, not only for maximizing microalgal carbohydrate accumulation, but also in terms of cost-effectiveness as the nutrient expenses for growing microalgae have typically accounted for approximately 25 % of the total microalgal production costs [11].

Therefore, the exploration of cost-effective approaches becomes a crucial factor in achieving a sustainable and practical large-scale green hydrogen production from microalgae [12]. Palm kernel expeller (PKE), a by-product generated by palm milling industries, emerges as a highly favourable alternative raw material source in Malaysia due to the extensive oil palm plantations that have inevitably produced substantial quantities of palm wastes. This low-cost waste biomass, characterized by its high carbohydrate composition [13], presents a significant potential as an organic carbon source for this study. However, a challenge to its practicality arises from its natural composition and complex lignin structure in which typically constituting around 20 %–40 % of its total composition. It is also cross-linking extensively with hemicellulose and cellulose structures; thereby these whole complex structures are not easily degraded [14].

Consequently, the pre-treatment process of lignocellulosic biomass is required to convert the stable biomass into fermentable sugars, which can be achieved through the disruption of rigid lignin and hemicellulose structures during hydrolysis [15]. Previous studies had shown that the photocatalytic pre-treatment process could selectively cleave the alkyl-aryl ether β-*O*-4 bonds found in lignin structure [16,17]. During the photocatalytic oxidation of lignin, the oxidative species generated by the photocatalyst surface such as $O_2^{\bullet-}$ and •OH react with lignin structure to form free radical cations, facilitating the breaking of C–C and C–O bonds in the β-*O*-4 bond structures [18]. Among the photocatalysts, TiO_2 has gained recognition as one of the most renowned and efficient options due to its various advantages, including low production cost, high thermal and chemical stability [19,20]. Various synthetic methods such as electrochemical, sol-gel, and hydrothermal treatment methods have been employed to produce one-dimensional TiO_2 nanotubes (NTs) [21,22]. Nevertheless, addressing the limitations of current fabrication methods, the TiO_2 nanostructures can be directly grown onto the substrate surface using electrochemical anodization procedure.

It is important to note that there is no research work has been performed so far in exploiting microalgae subsisting on TiO_2 NTs photocatalytic pre-treated PKE for green hydrogen production in which had appeared as the prime objective of this study. Accordingly, the TiO_2 NTs were employed for the pre-treatment of PKE, benefiting from their enhanced photoactivities under visible light irradiation. Moreover, the direct growth of NTs onto substrate surface had also facilitated the convenience of catalyst recovery upon the pre-treatment. Experimental investigations were conducted using different synthesized conditions of TiO_2 NTs' photocatalysts, including variations in electrolyte types and anodization voltages, to assess their effects on the pre-treatment of PKE and the subsequent release of soluble organic compounds for microalgal hydrogen production. Accordingly, it is crucial to optimize the condition of photocatalyst synthesis to achieve the enhanced microalgal hydrogen production upon subsisting on pre-treated PKE.

2. Materials and methods

2.1. Palm kernel expeller preparation and microalgae stock cultivation

Palm kernel expeller (PKE) was initially procured from a local palm oil mill, namely, United Fleet Palms Sdn. Bhd. located in Perak, Malaysia. The collected PKE sample was subjected to sieving using a sieve shaker to achieve the desired particle size of 2 mm [23]. The sieved PKE was stored in a closed container at room temperature until it was utilized for the pre-treatment study. The microalgal species of *Chlorella vulgaris*, obtained from the culture collections of Centre for Biofuel and Biochemical Research (CBBR), Universiti Teknologi PETRONAS, was used as the microalgal seed. A 500 mL volume of microalgal seed was cultured in a 5-L glass photobioreactor. The culture was continuously aerated with a compressed air at the rate of 6.5 L/min, and the ambient temperature was maintained at 25 ± 1 °C. The culture was also illuminated with a cool-white fluorescent lamp, providing a light intensity of 60–70 μmol/m^2s. Throughout the cultivation period, the pH was maintained at 7.0 ± 0.1 in a 4.5 L tap water-based medium containing KH_2PO_4 (0.7875 g/L), K_2HPO_4 (0.3375 g/L), and $NaNO_3$ (0.25 g/L). This microalgal stock, deprived of sulphur compounds, was cultured for 14 days to reach the stationary growth phase, prior to its use in the experiments.

2.2. Synthesis of TiO_2 nanotubes photocatalyst

A technical grade Ti foil (Ti Gr5/Tc4 Grade 5 ASTM B265) with a thickness of 0.1 mm was cut into a rectangular area with the dimension of 2 cm × 1 cm to serve as the working substrate at the anode. A Pt rod was utilized as the cathode for the anodization process. Prior to anodization, the Ti substrate underwent ultrasonic washing in acetone (99.5 %, Merck) for 10 min, followed by thorough rinsing with deionized water and air-drying. Subsequently, a mixture of choline chloride (ChCl, 99 %, Sigma Aldrich) and a hydrogen bond donor (HBD) was synthesized. The ChCl and HBD were mixed in a mole ratio of 1:2 and stirred under heating at 80 °C until a homogeneous, colourless liquid was formed [24]. The HBD used in this study were glycerol (Gly, 85 %, Merck), ethylene glycol (EG, 99.8 %, Merck), and urea (U, 99 %, Merck). These synthesized electrolytes were denoted as ChCl-Gly, ChCl-EG and ChCl-U, respectively.

The electrodes were immersed in 35 mL of electrolyte solution with the distance of 2.5 cm between the cathode and anode. The experiment was conducted at anodization voltages of 25 V, 30 V, and 35 V for a duration of 1 h at room temperature using each synthesized electrolyte. Upon completion of the anodization experiments, the samples were promptly removed from the electrolyte solution and rinsed with distilled water. Subsequently, the samples were air-dried at room temperature and calcined at 300 °C for 2 h. The mass of the photocatalyst obtained was calculated by weighing the sample after the anodization process, which was varied in the range of 0.08–0.09 g.

The surface morphology was examined using field emission scanning microscopy (FESEM, Carl Zeiss, SUPRA 55VP) and elemental composition of the reported nanotubes was determined using energy dispersive X-ray spectroscopy (AZtecOne, Oxford Instruments). Meanwhile, the crystalline structure was analysed using an x-ray diffractometer (XRD, PANalytical X'Pert3 Powder). Raman study was conducted using Hi-

Tech Instrument Model Horibba HR800 operating at 532 nm. The optical properties of the synthesized samples were evaluated using photoluminescence (PL) emission spectroscopy (Horiba LabRam HR Evolution). The diffuse reflectance UV–Visible (DRUV-Vis) spectrum of the sample was acquired using UV–Vis spectrometer (Agilent Carry100). The bandgap energy of TiO_2 NTs photocatalyst was determined from the reflectance data using Kubelka-Munk function and Tauc's plot according to the following equation:

$$\left[F(R).hv\right]^{1/2} = K\left(hv - E_g\right) \quad (1)$$

where K is the constant, h is the Plank's constant, v is the frequency of photon energy and E_g is the optical bandgap energy.

The valence band and conduction band of the TiO_2 NTs were calculated from combined DRUV-Vis and XPS results using the following equations:

$$E_{VB} = X - E_C + 0.5\,E_g \quad (2)$$

$$E_{CB} = E_{VB} - E_g \quad (3)$$

where X is the absolute electronegativity of TiO_2 (5.81 eV), E_c is the energy of free electrons (4.5 eV vs Normal Hydrogen Electrode) and E_g is the bandgap energy estimated using Equation (1).

2.3. Photocatalytic pre-treatment of palm kernel expeller

The photocatalytic pre-treatment was carried out by immersing the synthesized TiO_2 NTs photocatalyst into 80 mL of distilled water containing 0.5 g of PKE. In this regard, the efficiency of the photocatalysts' anodization voltages for each electrolyte was evaluated. The solution was stirred using a magnetic stirrer at 200 rpm and exposed to visible light using a 500 W halogen lamp for a duration of 3 h. After the completion of the pre-treatment study, a 3 mL liquid sample was extracted to assess the effects of pre-treatment duration, anodization voltage, and electrolyte solution on the soluble chemical oxygen demand (SCOD) and biochemical oxygen demand after 5 days (BOD_5) released by PKE disintegration. The liquid sample obtained after pre-treatment was then used for further microalgal hydrogen production studies. Each experimental setup was performed with a minimum of two replications to ensure the consistency of the results being attained.

2.4. Hydrogen production from microalgae subsisting on pre-treated palm kernel expeller

Hydrogen production study was carried out using pre-treated PKE at different anodization voltages in each of the ChCl-Gly, ChCl-EG and ChCl-U electrolyte solutions. The microalgal hydrogen production was conducted in a 200-mL serum bottle containing the mixture of 0.5 g of PKE in the solution after the pre-treatment process, and added with microalgal stock to attain a total working volume of 100 mL with an initial microalgal concentration of 0.25 g/L. Previously, preliminary study was conducted for several microalgal concentrations ranging from 0.10 to 0.50 g/L. It was found that 0.25 g/L of microalgal concentration was the minimum concentration required to effectively produce hydrogen.

Accordingly, this had left the bottle's headspace capacity at 100 mL. Prior to data collection, the solution underwent a 20-min purging process with nitrogen gas to create an anaerobic environment within the bottle. Subsequently, the bottle was sealed and continuously shaken in a dark environment at 150 rpm. The hydrogen produced was analysed at 24-h intervals until the production reached a plateau state. For analysis, a 1 mL volume of the headspace gas was withdrawn using a gas-tight syringe through a silicon septum cap positioned on top of the serum bottle. To ensure the consistency of the microalgal hydrogen production results, each setup was duplicated at least once.

2.5. Analytical methods

The analysis of SCOD was conducted following the Standard Methods APHA5520C (Closed reflux, titrimetric method). Concisely, a COD tube was prepared by adding 1.5 mL of standard potassium dichromate digestion solution and 2.5 mL of filtered sample. Then, 3.5 mL of sulfuric acid reagent (H_2SO_4) was introduced into the tube. The tube was securely capped and inverted several times to ensure thorough mixing. Subsequently, the COD tube was placed in a pre-heated block digester (Hach DRB200) set to 150 °C for a reflux period of 2 h. After cooling the COD tube to room temperature, the sample was titrated with a standard ferrous ammonium sulfate titrant (FAS). Prior to titration, 2 drops of ferroin indicator were added to the sample. The endpoint was determined by a sharp colour change from blue-green to reddish-brown. Similarly, a blank sample containing reagents and an equal volume of distilled water underwent reflux and titration. The SCOD was calculated using the following equation:

$$\text{SCOD (mg/L)} = \frac{(A - B) \times M \times 8000}{2.5\text{ mL sample}} \quad (4)$$

where A is the volume of FAS used for blank (mL), B is the volume of FAS used for sample (mL) and *M* is the molarity of FAS used.

The BOD_5 was measured according to the Standard Methods APHA5210B for the samples of pre-treated PKE. The dilution water was prepared by a continuous aeration for 24 h prior to use. The samples were placed in airtight BOD bottles and incubated at 20 °C ± 1 °C in the incubator (FOC 120E, PLT Scientific) for five days with no lights to prevent the algal growth. A small amount of microorganisms of the seed from the sewage sludge was introduced to each tested sample. The dissolved oxygen concentrations before and after the incubation period were measured using a dissolved oxygen meter (YSI 5100). The control was prepared by adding dilution water and equal volume of seed. The BOD_5 was calculated according to the following equation:

$$\text{BOD (mg/L)} = \frac{(D_0 - D_f) - f(B_0 - B_f)}{P} \quad (5)$$

where D_0 is the initial dissolve oxygen in the sample mg/L, D_f is the final dissolve oxygen in the sample after the incubation period of five days mg/L, B_0 is the initial seeded dissolve oxygen in control mg/L, B_f is the final seeded dissolve oxygen in control mg/L, f is the fraction of seed in the incubated sample and P is the fraction of the incubated sample.

The hydrogen gas sample extracted into a gas-tight syringe was promptly injected into the gas chromatography-thermal conductivity detector (GC-TCD) unit. The unit was equipped with a molecular sieve 5A column, and helium gas was used as the carrier gas at a constant flow rate of 35 mL/min. The packed column was maintained at a temperature of 110 °C, while the thermal conductivity detector was set at 200 °C. The volume of hydrogen gas presented in the 1 mL gas sample was determined from the calibration curve prepared from known volumes of hydrogen gas.

3. Results and discussion

3.1. Photocatalytic pre-treatment of palm kernel expeller

The investigation aimed to assess the efficacy of photocatalytic pre-treatment of palm kernel expeller (PKE) in converting its particulate organic matters into the soluble phase. This assessment was conducted by measuring the concentrations of soluble chemical oxygen demand (SCOD) and biochemical oxygen demand after 5 days (BOD_5). The results are presented in Fig. 1 in demonstrating the impacts of different anodization voltages and electrolyte types on PKE after the pre-treatment duration of 3 h. Generally, the SCOD concentrations showed an increasing trend for all PKE samples being pre-treated with increasing anodization voltages from each electrolyte. Among the TiO_2 NTs

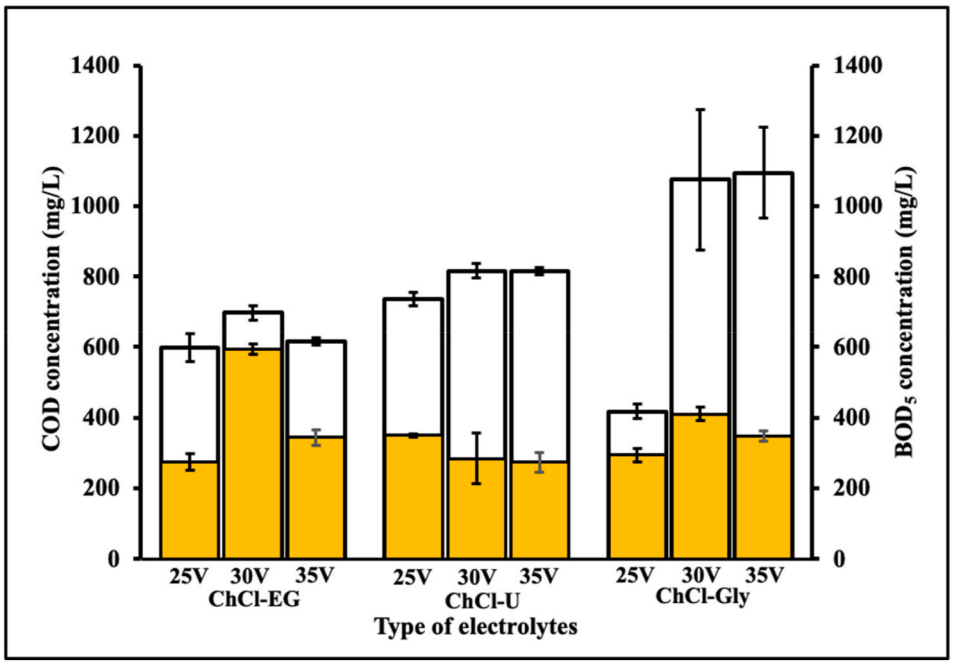

Fig. 1. SCOD and BOD_5 concentrations generated by photocatalytic pre-treated PKE synthesized at different anodization voltages and electrolytes. Each bar chart represents the total SCOD concentration with yellow colour portion within every bar chart signifying the BOD_5 concentration. (For interpretation of the references to colour in this figure legend, the reader is referred to the Web version of this article.)

photocatalysts that were synthesized in ChCl-EG electrolyte, the highest SCOD concentration of 607 mg/L was observed for the anodization voltage of 30 V, followed by a slight decline at higher voltage. This observation suggested that the pre-treatment process had disrupted the lignin structure within the PKE, leading to the increase in soluble organic concentrations in the liquid phase, i.e., the formation of soluble, easily biodegradable fractions [25]. The decrease in SCOD concentration at high anodization voltage of 35 V may be attributed to the immediate mineralization of intracellular substances by the highly oxidative hydroxyl radicals that were generated during the degradation process, resulting in the loss of organics from the PKE substrate [26].

On the other hand, the SCOD concentrations had remained relatively stable for photocatalysts being synthesized in ChCl-U and ChCl-Gly electrolytes after reaching the anodization voltage of 30 V, with SCOD concentrations of around 816 mg/L and 1075 mg/L, respectively. Notably, the differences were measured in terms of BOD_5 concentrations derived from PKE pre-treated using photocatalysts synthesized in ChCl-U and ChCl-Gly electrolytes. The PKE pre-treated at 25 V with ChCl-U exhibited higher BOD_5 concentration than other high voltages' pre-treatments, which was contrasting with its SCOD concentrations. Moreover, the PKE pre-treated with TiO_2 NTs synthesized in ChCl-Gly had exuded much lower BOD_5 concentrations as opposed to its total SCOD concentrations for the respective 30 V and 35 V pre-treated PKE's samples. These signified that the released organic compounds from PKE were not easily degraded after the photocatalytic pre-treatment although the values of SCOD were very high for both anodization voltages.

Previous studies had highlighted the limited potential of microalgal feedstock used for producing green hydrogen; primarily due to the low availability of soluble organic contents which was relying on the effectiveness of its biomass hydrolysis process. Maryam et al. [26] and Qiao et al. [27] had both reported that the increase in SCOD concentrations could enhance the biogas production. Therefore, the hydrogen production study was conducted to assess the digestibility of pre-treated PKE at various anodization voltages and electrolyte types as depicted in Fig. 2. Observing from this figure, it could be noted that the PKE pre-treated at 30 V using ChCl-EG, ChCl-U and ChCl-Gly electrolytes had resulted in the highest hydrogen yields, being measured at 142, 94, and 43 mL/g SCOD, respectively. In fact, the microalgal hydrogen yield from ChCl-EG electrolyte had aligned well with the BOD_5 concentration (Fig. 1). This pre-treatment process had facilitated a greater release of biodegradable organic materials as compared with PKE pre-treated at 25 V and 35 V using the same type of electrolyte as well as other pre-treated PKE's samples. Conversely, PKE pre-treated at 25 V and 35 V in ChCl-Gly electrolyte demonstrated the lowest hydrogen yields among the different electrolytes, recorded at merely 10 and 18 mL/g SCOD, respectively. Despite having high SCOD concentrations, especially the PKE's sample from 35 V, all the samples exhibited low levels of biodegradable organic materials in which had likely contributed to their reduced hydrogen yields.

The enhancement of hydrogen yields could be justified by the photocatalytic pre-treatment process which had served the purpose of depolymerizing the lignin in PKE substrate while releasing the highly biodegradable organic compounds. This finding aligned with previous studies that had demonstrated the successful degradations of lignin, and subsequent enhancement of biogas productions through photocatalytic pre-treatment processes. For instance, Alvarado-Morales et al. [28] investigated the photocatalytic degradation of wheat straw utilizing TiO_2, and thereafter, achieving an augmented production of biogas. Similarly, Corro et al. [29] examined the photocatalytic degradation of coffee pulp using 10 % Cu/TiO_2 as the highly efficient photocatalyst. The authors had recorded the increased amounts of methane, propane, and other combustible components in the biogas generated. Another study by Tedesco et al. [30] explored the effect of photocatalytic pre-treatment using TiO_2 supported by natural zeolites on *Miscanthus giganteus* (also known as elephant grass); and also observed the enhancement of biogas production being achieved. These studies had collectively highlighted the crucial role of increasing soluble organic matters through the photocatalytic pre-treatments, as the release of degradable organic compounds form the fundamental steps was important for efficient biogas productions [25].

Fig. 3 demonstrates the relationship between hydrogen productions from microalgae and BOD_5 concentrations generated by pre-treated PKE at different anodization voltages and electrolytes. When the PKE was

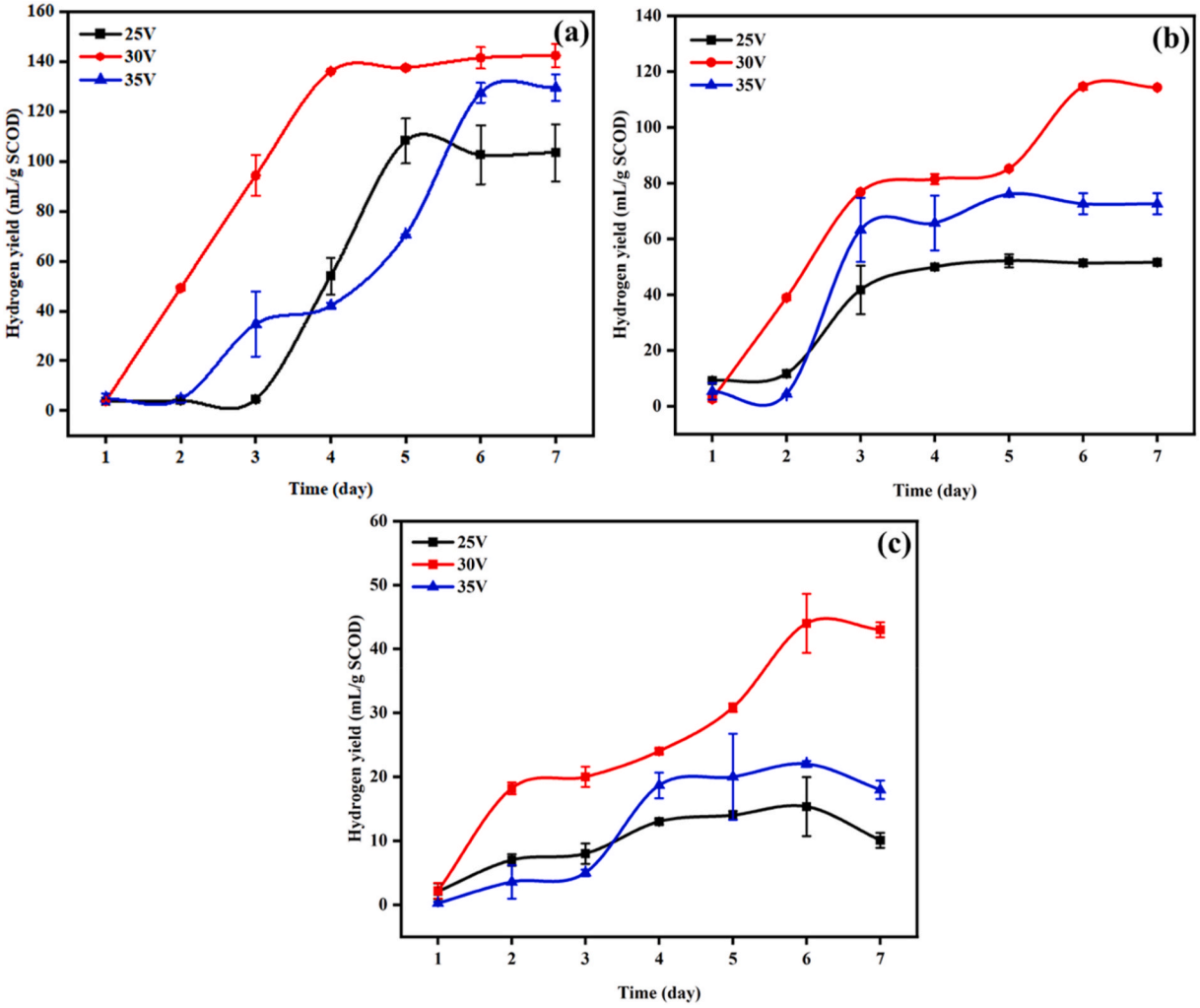

Fig. 2. Microalgal hydrogen yields subsisting on photocatalytic pre-treated PKE synthesized at different anodization voltages and electrolytes: (a) ChCl-EG, (b) ChCl-U and (c) ChCl-Gly.

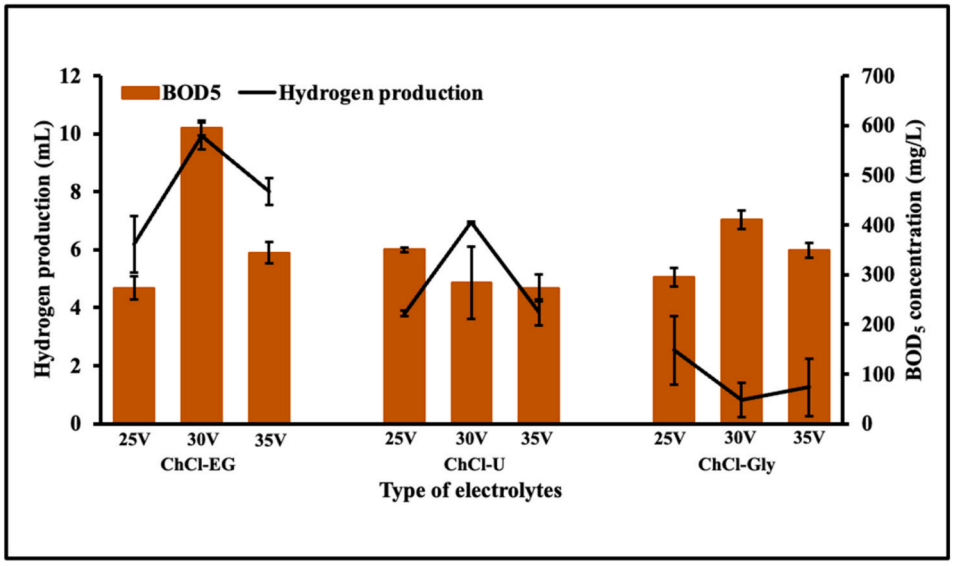

Fig. 3. Hydrogen productions in relation to BOD_5 concentrations generated by photocatalytic pre-treated PKE synthesized at different anodization voltages and electrolytes.

pre-treated by TiO_2 NTs synthesized at 25, 30, and 35 V in ChCl-EG electrolyte, the corresponding total hydrogen gas volumes generated were 6, 10, and 8 mL. In contrast, the pre-treated PKE at the same voltages in ChCl-U electrolyte had resulted in the total hydrogen productions of 4, 7, and 4 mL, respectively. Accordingly, the highest values were achieved at 30 V for both electrolytes. On the other hand, the trend observed for total hydrogen productions in ChCl-Gly electrolyte was showing a continuous decrease from 2.5 to 1.2 mL at the respective anodization voltages from 25 to 35 V. Indeed, the lowest hydrogen productions as opposed to the former electrolytes employed. These findings highlighted the impact of both electrolyte compositions and voltages on hydrogen generations with varying trends in total hydrogen gas productions at different anodization voltages. Also, the BOD_5 concentrations released by photocatalytic pre-treated PKE in different electrolytes could be directly proportionated to microalgal hydrogen productions better than the SCOD concentrations. For instance, the highest BOD_5 concentrations derived from pre-treated PKE in ChCl-EG electrolyte had led to the highest microalgal hydrogen productions. However, the measured SCOD concentrations (Fig. 1) were inappropriately the lowest for ChCl-EG among the electrolytes employed.

In this regard, as can be seen in Fig. 4, the PKE pre-treated by TiO_2 NTs synthesized in ChCl-EG electrolyte had shown the highest positive correlation between generated BOD_5 concentrations and microalgal hydrogen productions in comparison with other electrolytes, namely, ChCl-U and ChCl-Gly. Overall, the ultimate correlation was following the sequence of ChCl-EG > ChCl-U > ChCl-Gly based on the volume of produced microalgal hydrogen per amount of BOD_5 accessible. As such, the use of ChCl-EG electrolyte had achieved the highest value of 251 mL-H_2/g-BOD_5 in which at 15 % and 75 % higher than the ChCl-U and ChCl-Gly electrolytes, respectively. This confirmed the aptness of using ChCl-EG electrolyte to synthesize TiO_2 NTs for pre-treating PKE especially at 30 V in generating the highest BOD_5 concentration, and later, the highest microalgal hydrogen production.

In further validating the impact of photocatalytic pre-treatment on PKE, the TiO_2 NTs photocatalyst synthesized at 30 V in ChCl-EG was employed for prolonged photocatalytic pre-treatment duration owing to its remarkable potential to enhance the microalgal hydrogen production as demonstrated in Fig. 2(a). The concentrations of both SCOD and BOD_5 in the pre-treated PKE are presented in Fig. 5. It was evident that the maximum SCOD concentration in the pre-treated PKE was observed after 2 h of pre-treatment duration, and gradually decreasing thereafter. Conversely, the BOD_5 concentration exhibited the significant increase at 3 h of pre-treatment duration with value being attained at 548 mg/L, followed by the subsequent gradual decline similar to SCOD. These findings heralded that the pre-treatment duration of 3 h was sufficient to release the highest biodegradable organic materials necessary for the subsequent hydrogen production by microalgae. However, it was worth noting that the BOD_5 concentrations decreased after 3 h of photocatalytic pre-treatment duration which may be attributed to the increase in lignin molecules being adsorbed onto photocatalyst surface. The adsorbed lignin molecules could result in blocking the active sites as well as reducing the generation of active species. Consequently, leading to the decrease of conversion efficiency to produce biodegradable organic compounds from PKE [31].

In accordance with the findings of Machado et al. [32], the degradation of lignin in the presence of the TiO_2 photocatalyst and light was believed to result from the synergistic actions of singlet oxygen, hydroxyl radicals, and superoxide radicals. These reactive species are typically the primary contributors in the photocatalytic process when oxygen was present. The following equations summarize the formation of radicals under photocatalytic conditions [32,33]. In this case, the S stands for the lignin substrate, while TiO_2 (h^+) and TiO_2 (e^-) represent the electron deficient and electron-rich parts in the structure of TiO_2, respectively.

$$TiO_2 \rightarrow TiO_2(e^- / h^+) \quad (6)$$

$$TiO_2(h^+) + H_2O \rightarrow TiO_2 + OH^{\bullet} + H^+ \quad (7)$$

$$TiO_2(h^+) + S \rightarrow TiO_2 + S^{+\bullet} \quad (8)$$

$$TiO_2(h^+) + OH^- \rightarrow TiO_2 + OH^{\bullet} \quad (9)$$

$$TiO_2(e^-) + O_2 \rightarrow TiO_2 + O_2^{-\bullet} \quad (10)$$

$$OH^- + O_2 \rightarrow OH^{\bullet} + O_2^{-\bullet} \quad (11)$$

$$OH^{\bullet} + O_2^{-\bullet} \rightarrow OH^- + {}^1O_2 \quad (12)$$

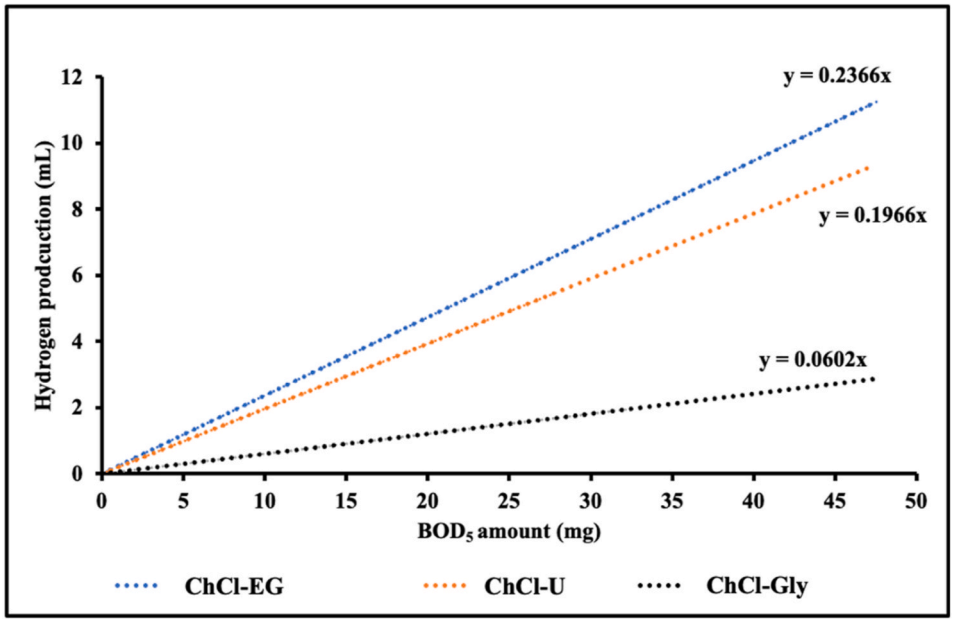

Fig. 4. Correlation between microalgal hydrogen productions and BOD_5 amounts generated by photocatalytic pre-treated PKE synthesied at different electrolytes.

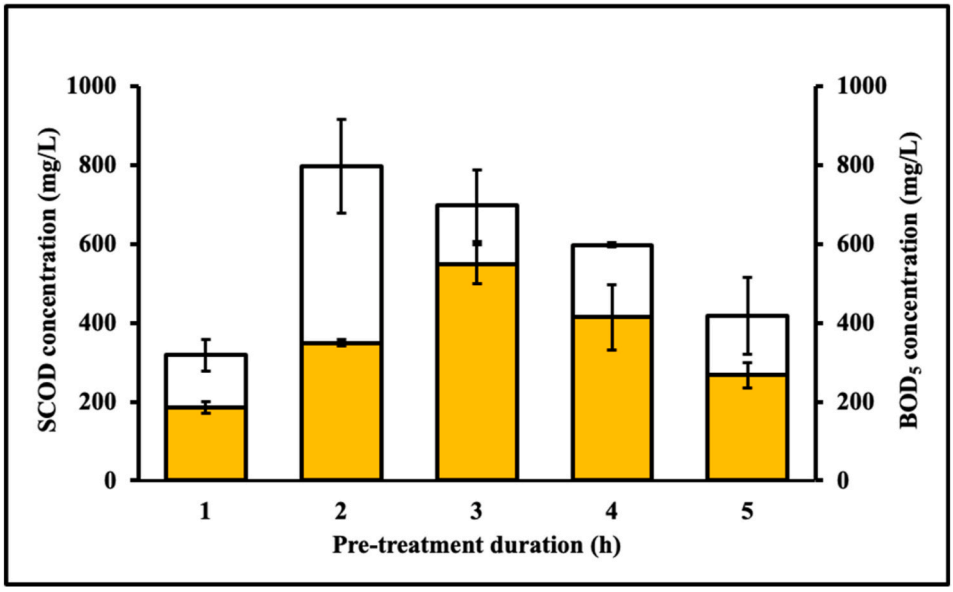

Fig. 5. SCOD and BOD_5 concentrations generated by photocatalytic pre-treated PKE synthesized at 30 V in ChCl-EG electrolyte. Each bar chart represents the total SCOD concentration with yellow colour portion within every bar chart signifying the BOD_5 concentration. (For interpretation of the references to colour in this figure legend, the reader is referred to the Web version of this article.)

3.2. Characterization of TiO_2 NTs

The photocatalysts used for characterization were TiO_2 NTs which were synthesized in ChCl-EG electrolyte at 25, 30, and 35 V. These TiO_2 NTs' samples because of its capabilities to enhance the microalgal hydrogen productions subsisting on pre-treated PKE, especially for the TiO_2 NTs synthesized at 30 V. The XRD patterns from TiO_2 NTs photocatalysts that were calcined for 2 h at 300 °C are shown in Fig. 6(a) in which illustrates the characteristic diffraction peaks of titanium metal (JCPDS 044–1294) at 35°, 38°, 40°, 52°, 63°, 71°, 76° and 77° in which corresponding to the (100), (005), (101), (102), (110), (103), (112) and (201) planes, respectively, indicating the formation of TiO_2 NTs. These observations were consistent with the previously reported studies [22,34,35]. It was worth noting that a low calcination temperature of 300 °C was considered desirable as it had the capability to transform the amorphous phase into an anatase phase structure, consistent with findings as reported by Yu and Wang [31] and Xiao et al. [33].

Additionally, the characteristic diffraction peak at $2\theta = 25°$ was

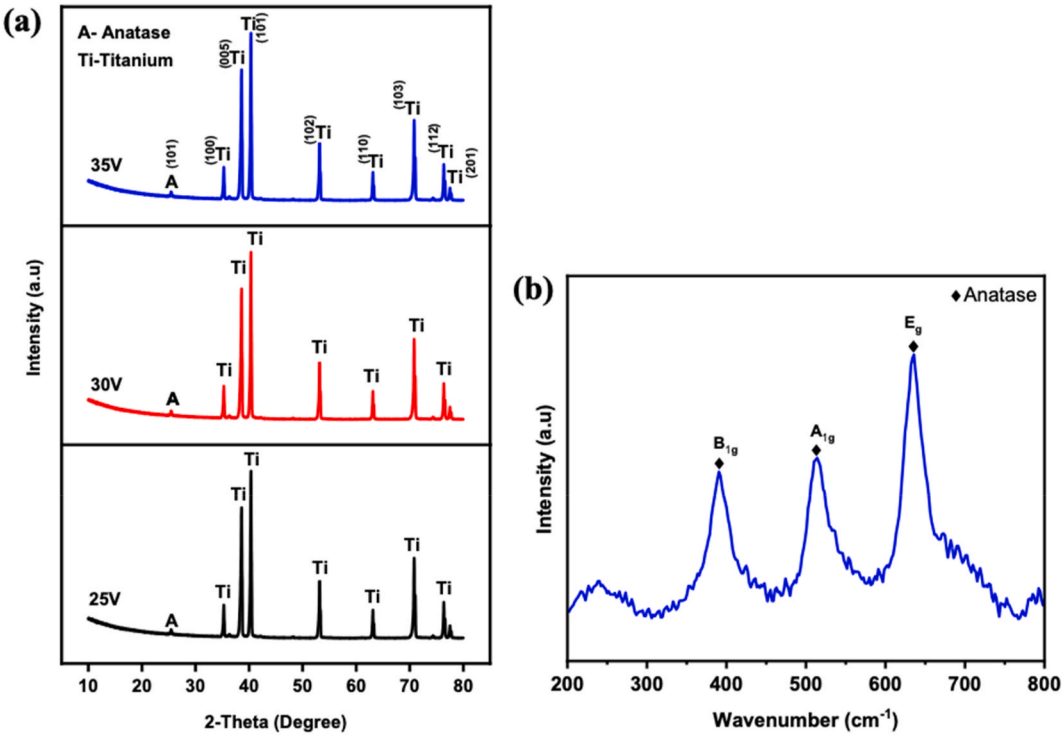

Fig. 6. (A) XRD patterns of TiO_2 NTs synthesized at various anodization voltages in ChCl-EG electrolyte and (b) RAMAN spectra of TiO_2 NTs synthesized at 30 V in ChCl-EG electrolyte.

corresponding to the (101) planes of the anatase phase (JCPDS 021–1272) which was also observed for all anodization voltages; in line with the study conducted by Liu et al. [36]. Moreover, the intensity of anatase peak was as well in good agreement with the research conducted by Erol et al. [37] who had investigated the effect of various anodization voltages. According to this finding, the anatase peak could be obtained even at low anodization voltages, e.g., 20 V, and the peak intensity was not significantly influenced by the anodization voltages.

The TiO_2 NTs photocatalyst synthesized at 30 V in ChCl-EG electrolyte underwent further structural analysis using Raman spectroscopy. The obtained spectrum validated the presence of solely anatase as the TiO_2 phase on the photocatalyst surfaces, as depicted in Fig. 6(b). Notably, distinct peaks at approximately 399 (B_{1g}), 516 (A_{1g}), and 639 cm^{-1} (E_g) were identified, corresponding to the characteristic Raman modes of anatase TiO_2 [38]. There was no evidence indicating a phase transition from anatase to rutile within the sample.

In addition, the physical structural morphology of TiO_2 NTs is strongly governed by the electrochemical condition, specifically the electrochemical voltage as it is the rudimentary aspect controlling the inner tube diameter [39]. Generally, the TiO_2 NTs' growth occur proportionally with the electrochemical voltage up to a threshold voltage in which the dielectric breakdown of oxide will transpire thereafter. The influence of anodization voltages on TiO_2 NTs formation was explored with the intention to fabricate NTs possessing an optimum pore diameter to enhance the photocatalytic pre-treatment of PKE under the visible light irradiation. Fig. 7 represents the FESEM images of TiO_2 NTs synthesized in ChCl-EG at various anodization voltages. The tubes formation was observed at 25, 30 and 35 V of anodization voltages with average tube diameters of 26.14 ± 1.30, 73.01 ± 1.94, and 122.00 ± 13.32 nm, respectively. The tube morphology for TiO_2 NTs prepared at 25 V had produced a poor ordered structure on the surface of Ti foil as can be observed in Fig. 7(a). Increasing the voltage to 30 V had formed a dense cluster of TiO_2 NTs as presented in Fig. 7(b). Accordingly, the numbers of NTs produced at 25 and 30 V also showed an increased trend from 5.07×10^9 to 6.28×10^9 tubes/cm^2, respectively. Nonetheless, it was crucial to note that the further increase in electrochemical voltage to 35 V had resulted to the rupture and disintegration of NTs. Therefore, less dense distribution of tubular structure was observed with only about 3.11×10^9 tubes/cm^2 were produced (Fig. 7(c)).

Furthermore, the average inner tube diameters had increased from 26.14 ± 1.30 to 122.00 ± 13.32 nm when the voltages were raised from 25 to 35 V, respectively. These results were in agreement with the findings reported by Omidvar et al. [40] who had concluded that the inner tube diameter was found to increase with increasing electrochemical voltage. This could be due to the intense electrical field dissolution in which accelerated the growth of pits during the early stage of electrochemical process. These pits were etched to form larger pores at the high anodization voltage. Moreover, at high anodization voltage, the disruption of tube morphology was as well observed because the rate of chemical dissolution was too high, causing imbalance in the reaction between the chemical dissolution and electrical field dissolution [41]. Another study had proposed that the variation in electrochemical voltage would determine the strength of electrical field being evolved across the oxide layer; and thus, affecting the tube diameter. Therefore, larger diameter NTs were developed at higher voltages [42]. Qin et al. [43] reported that the NTs with diameters ranging between 30 and 90 nm could be fabricated by electrochemical anodization in 0.25 wt% of NH_4F^+ ethylene glycol solution with 2 vol% of water at the voltages between 30 and 60 V, respectively. Also, Gong et al. [44] showed that the increase of TiO_2 NTs diameter could be acquired from 25 to 65 nm for anodization voltages ranging from 10 to 40 V, respectively, when Ti foils were anodized in 0.5 wt% of HF solution. All these studies vindicated that the NTs diameter is greatly affected by the electrochemical anodization voltage. On another note, the rates of PKE in releasing the BOD_5 upon being pre-treated by TiO_2 NTs synthesized at 25, 30 and 35 V were 5.83×10^{-2}, 5.86×10^{-2}, and 0.77×10^{-2} mg-BOD_5/cm^2-TiO_2 NTs surface s, respectively. These results confirmed that the release of organic materials from lignocellulosic PKE was highly influenced by anodization voltage, in which the 30 V had attained an optimum total surface area of TiO_2 NTs for maximizing the generation of BOD_5 in the enhancement of microalgal hydrogen production.

The energy dispersive X-ray spectroscopy (EDX) spectrum of the

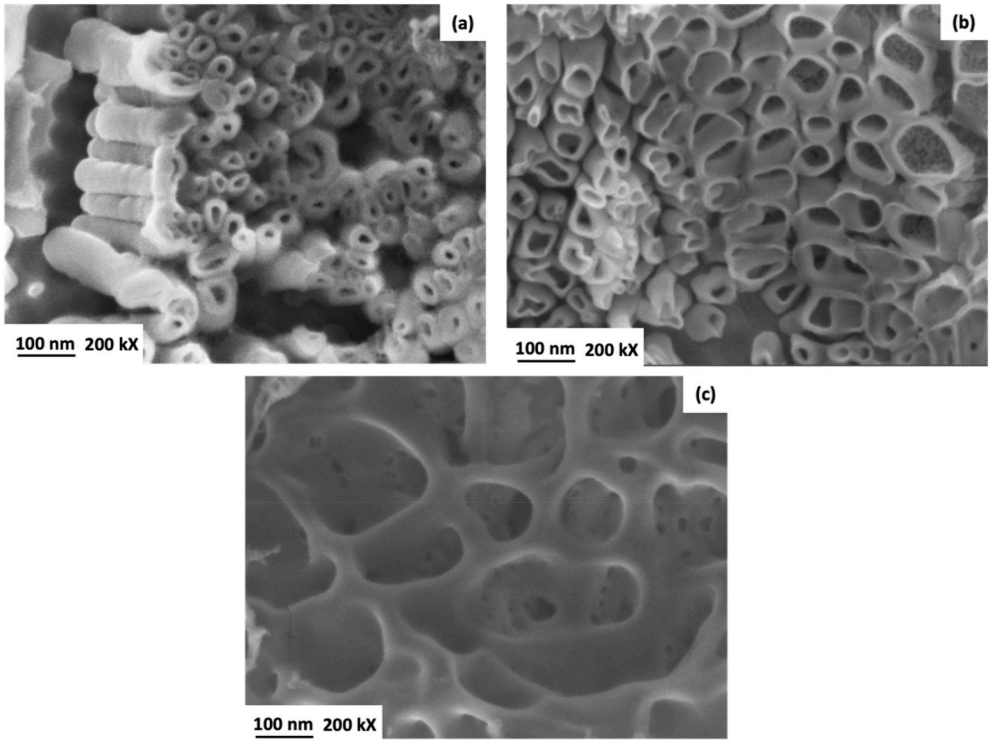

Fig. 7. FESEM images of TiO_2 NTs synthesized in ChCl-EG electrolyte at 25 (a), 30 (b), and 35 (c) V.

synthesized TiO_2 NTs at 30 V is presented in Fig. 8. This figure shows that the TiO_2 NTs had been successfully synthesized with the presence of only Ti and O elements in the sample with no sign of impurity from other element. The bandgap energy of TiO_2 NTs photocatalyst synthesized at 30 V in ChCl-EG electrolyte was determined from reflectance data using Kubelka-Munk function and Tauc's plot. Fig. 9(i) depicts Tauc's plot of $[FR.hv]^{1/2}$ versus hv. The bandgap energy was calculated by extrapolating the linear portion of the curve to intercept energy axis and was found to have a value of 2.74 eV. The valence band and conduction band values were 2.68 and −0.06 eV, respectively. According to Nawaz et al. [45], the band structure suggested that the electron (e^-) TiO_2 NTs photocatalyst could be easily photoexcited from the valence band to the conduction band, accompanied by superior charge carriers separation using visible light. The key findings from DRUV-Vis investigation included the significant visible light absorption resulted from the low bandgap (<3.0 eV) as observed in the synthesized material.

The photoluminescence (PL) spectrum of TiO_2 NTs was also obtained to study the optical property and behavior of electron-hole recombination. The photocatalytic activity of TiO_2 depended largely on the lifespan of photogenerated electrons and holes on its surface. The emission spectra of TiO_2 NTs synthesized at 30 V in ChCl-EG, ChCl-U and ChCl-Gly were in the visible light wavelength range of 350–700 nm as shown in Fig. 9(ii). The main emission peaks for TiO_2 NTs had appeared at 386 nm (3.21 eV), 520 nm (2.38 eV), and 545 nm (2.28 eV). The peak at 386 nm was referred to the near band edge emission of TiO_2, corresponding to the bandgap energy of anatase phase of TiO_2 [46]. Generally, the anatase is regarded as more photochemically active phase of TiO_2 NTs due to its lower electron-hole recombination rate and higher surface adsorptive capacity [47]. The PL peak intensities of the photocatalyst synthesized in ChCl-EG showed a significant decrease as compared with samples prepared in ChCl-U and ChCl-Gly. The lowest PL intensity revealed that the photo-generated holes and electrons had the lowest recombination rate in the sample. The improved microalgal hydrogen production as observed for the TiO_2 NTs photocatalyst synthesized at 30 V in ChCl-EG may be attributed to the enhanced absorption in visible light, consequently facilitating more effective separation of electron-hole pairs.

3.3. Stability of recycled TiO_2 NTs photocatalyst

Recyclability plays a crucial role in photocatalysis as it determines the stability and efficiency of photocatalyst over multiple cycles of uses. The industrial viability is greatly enhanced if the efficiency of photocatalyst does not decrease significantly with each cycle of reusing [48]. In this study, the TiO_2 NTs photocatalyst was chosen due to its direct growth on Ti foil potential, which improves the electron transfer pathways, enhances the photon absorptions, and enriches the extensive adsorptions of reactant molecules onto photocatalyst's surface [49,50]. Based on the superior performance, the TiO_2 NTs anodized at 30 V in ChCl-EG electrolyte was reused for four consecutive cycles. Accordingly, the spent TiO_2 NTs was rinsed with distilled water and reused in the subsequent cycle without any further treatment. The recyclability assessment results in terms of BOD_5 releases from pre-treated PKE that eventually affected the microalgal hydrogen productions are presented in Fig. 10. The photocatalytic pre-treatment of PKE exhibited a decreasing trend in BOD_5 concentration with values of 594.32, 360.82, 357.82, and 354.82 mg/L from cycle 1 to 4, respectively. It was evident that the photocatalytic activity had experienced a reduction of approximately 40 % from cycle 1 to 2. However, the reduction of activity had tapered off thereafter, i.e., the photocatalytic activity was successfully maintained with only a reduction of 2 % from cycle 2 to 4. Overall, the photocatalytic activity was well retained throughout the recycling process from cycle 2 onwards. According to the research conducted by Weon et al. [51], the deactivation of TiO_2 photocatalyst primarily occurred due to the accumulation of carbonaceous intermediates onto its surface. Furthermore, Wint et al. [52] reported that the carbon contaminants likely originated from the adsorption of hydrocarbons during the recycling experiments. As observed in the current recycling study, it was confirmed that the synthesized TiO_2 NTs photocatalyst could be feasibly reused in repeated cycles for the photocatalytic pre-treatment of PKE. Subsequently, the pre-treated PKE from each individual cycle was employed to evaluate the microalgal hydrogen productions as shown in Fig. 10. In this regard, a steep reduction in hydrogen productions was recorded during the cycle 1 to 2 due to the tremendous decrease in photocatalytic activity that had prompted the 40 % flop in BOD_5 release. Starting from cycle 2 onwards, the production of hydrogen by microalgae had only experienced a slight drop in terms of volumes, indicating the high level of stability of synthesized TiO_2 NTs photocatalyst in ChCl-EG electrolyte at 30 V.

Further analysis of BOD_5 consumed by microalgae during the production of hydrogen for each cycle is depicted in Fig. 11. The BOD_5 consumed by microalgae during the cycle 1 was measured at 394 mg/L, followed by 261, 256, and 246 mg/L for the cycle 2 to 4, respectively. Additionally, the efficiencies of BOD_5 conversion to hydrogen were exhibiting an increasing trend until the cycle 2 before plateauing from cycle 3 onwards. Indeed, the microalgal hydrogen production volume

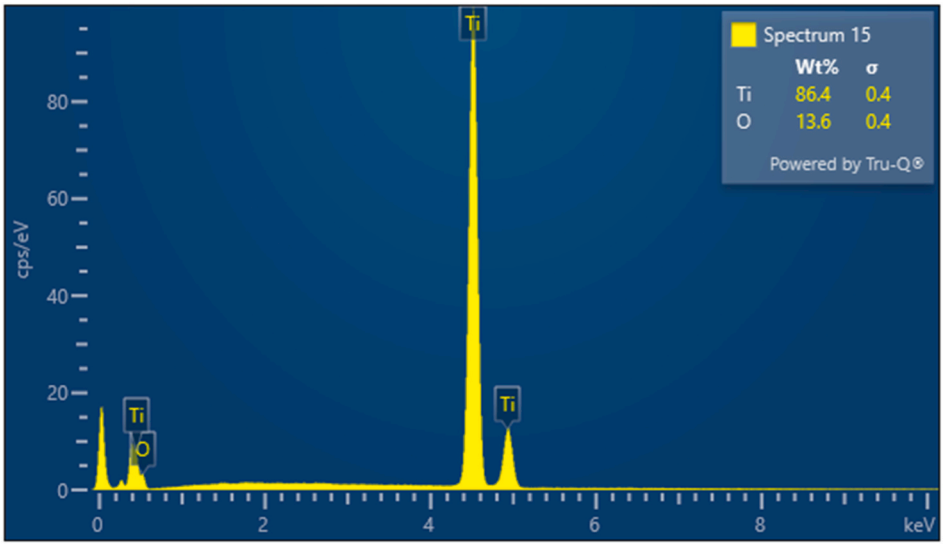

Fig. 8. EDX spectrum of TiO_2 NTs synthesized in ChCl-EG electrolyte at 30 V.

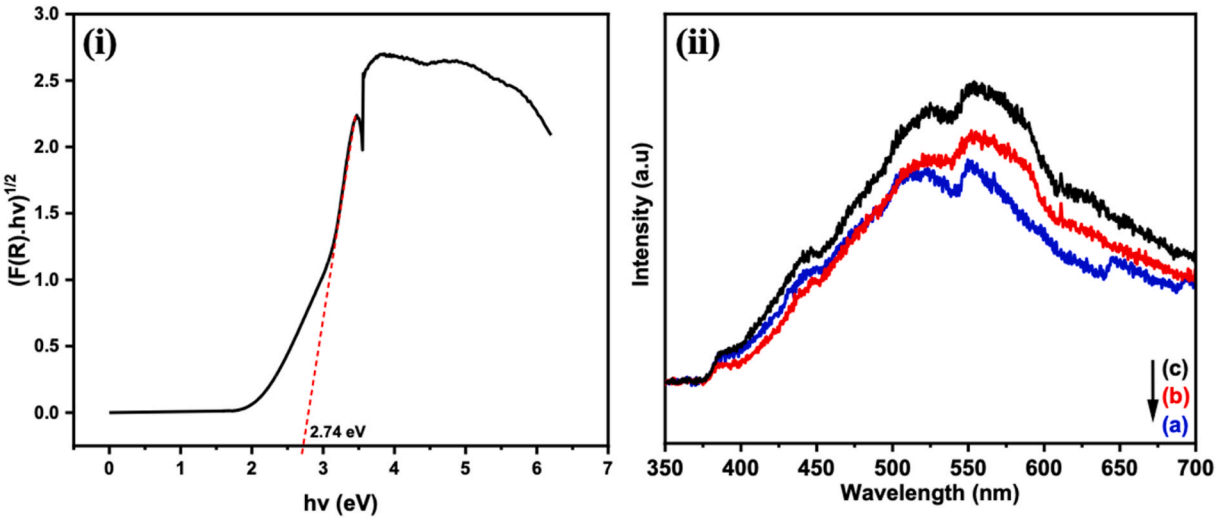

Fig. 9. (i) Tauc plot calculated using the Kubelka-Munk function for TiO_2 NTs synthesized at 30 V in ChCl-EG electrolyte and (ii) PL spectrum of TiO_2 NTs synthesized at 30 V in different electrolytes: (a) ChCl-EG, (b) ChCl-U and (c) ChCl-Gly.

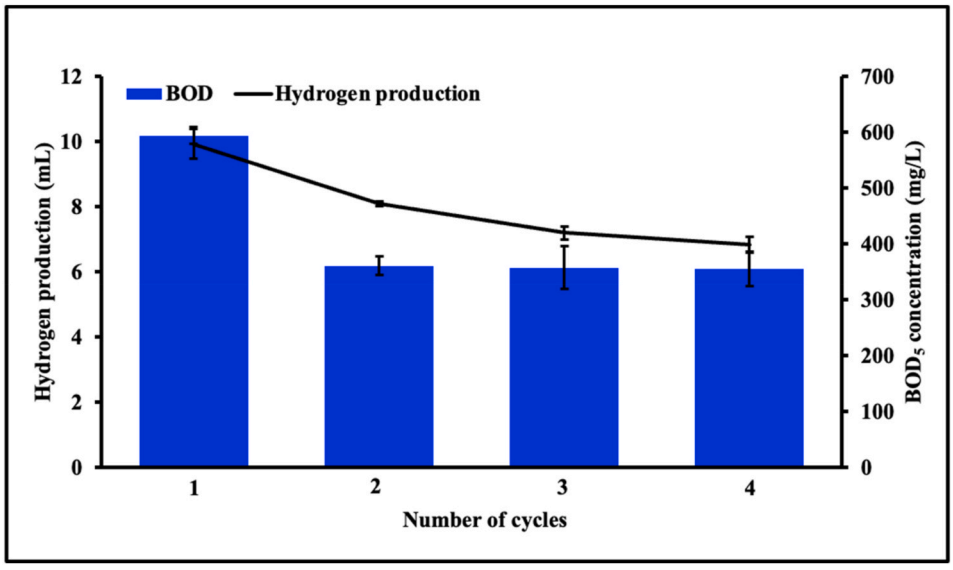

Fig. 10. Recyclability of TiO_2 NTs synthesized in ChCl-EG electrolyte at 30 V, and subsequently, used for the pre-treatment of PKE in production microalgal hydrogen.

after four consecutive cycles had shown the reduction of almost 30 %, with the 27 % decrease transpiring in cycle 3 as compared with cycle 1. This evidenced that the photocatalytic activity was well maintained from cycle 3 onwards with only about 3 % decrease in microalgal hydrogen production while comparing between cycle 3 and 4 using recycled TiO_2 NTs photocatalyst synthesized in ChCl-EG electrolyte at 30 V.

4. Conclusions

TiO_2 NTs were successfully synthesized for all anodization voltages and different types of electrolytes via electrochemical anodization of Ti foil in this study. The characteristic diffraction peak at $2\theta = 25^\circ$ corresponding to the (101) planes of the anatase phase were observed for sample synthesized in ChCl-EG electrolytes. Raman spectra further confirmed the presence of solely anatase as the TiO_2 phase on the photocatalyst surfaces and supported by SEM/EDX showing the presence of Ti and O elements in the samples. Photocatalytic pre-treatment of PKE employing TiO_2 NTs photocatalyst anodized in ChCl-EG at 30 V was found best as it had yielded the highest concentration and releasing rate of biodegradable organic materials measured at 594 mg/L and 5.86 $\times 10^{-2}$ mg-BOD_5/cm^2-TiO_2 NTs surface s, respectively. Significant enhancement of hydrogen yield with value at 142 mL/g-SCOD was also achieved. The photocatalytic pre-treatment of PKE exhibited a gradual decreasing trend in BOD_5 concentrations with values of 594.32, 360.82, 357.82, and 354.82 mg/L after four consecutive cycles of repeatedly utilizations, respectively. Nevertheless, the efficiency of BOD_5 conversion into microalgal hydrogen was well maintained even after four consecutive cycles with only 9 % reduction in comparing with first cycle. Accordingly, this green hydrogen production is sustainable through waste PKE reduction-cum-conversion as mediated by fermentative microalgae.

Declaration of competing interest

The authors declare that they have no known competing financial interests or personal relationships that could have appeared to influence

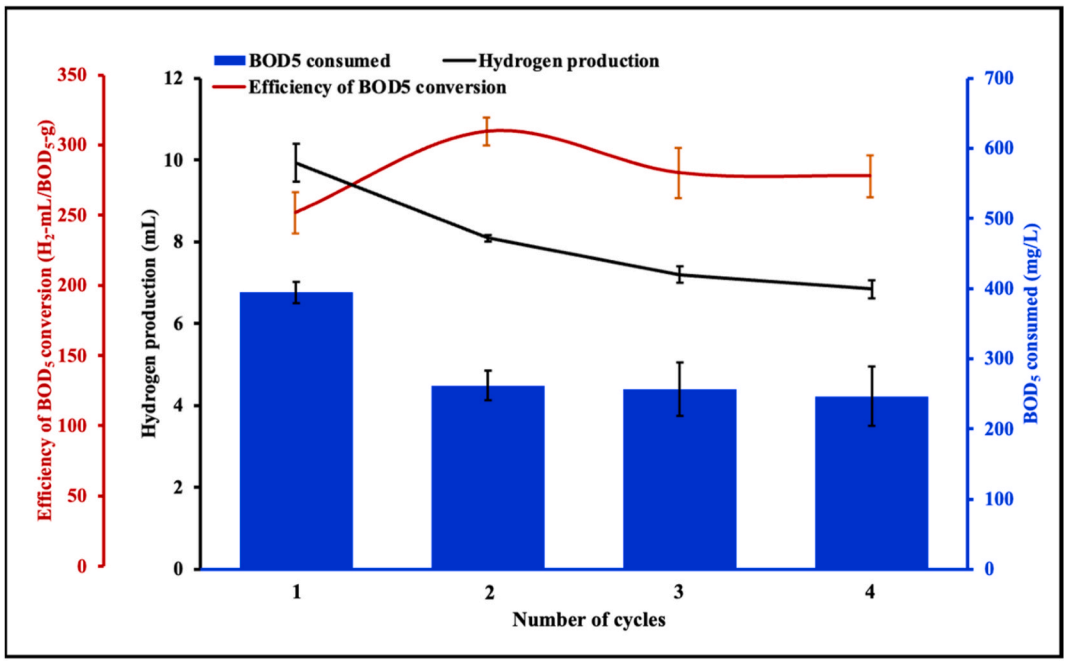

Fig. 11. Efficiency of BOD_5 conversions into microalgal hydrogen using recycled TiO_2 NTs synthesized in ChCl-EG electrolyte at 30 V for the pre-treatment of PKE.

the work reported in this paper.

Acknowledgements

The financial support received from YUTP-FRG with the cost centre of 015LC0-495 is gratefully acknowledged. This work was funded by the Researchers Supporting Project Number (RSPD2023R672) King Saud University, Riyadh, Saudi Arabia.

References

[1] Catumba BD, Sales MB, Borges PT, Ribeiro Filho MN, Lopes AAS, Sousa Rios MA de, et al. Sustainability and challenges in hydrogen production: an advanced bibliometric analysis. Int J Hydrogen Energy 2023;48:7975–92. https://doi.org/10.1016/j.ijhydene.2022.11.215.

[2] Li S, Chang H, Zhang S, Ho S-H. Production of sustainable biofuels from microalgae with CO2 bio-sequestration and life cycle assessment. Environ Res 2023;227:115730. https://doi.org/10.1016/j.envres.2023.115730.

[3] Derwent RG. Global warming potential (GWP) for hydrogen: sensitivities, uncertainties and meta-analysis. Int J Hydrogen Energy 2023;48:8328–41. https://doi.org/10.1016/j.ijhydene.2022.11.219.

[4] Nagarajan D, Lee D-J, Kondo A, Chang J-S. Recent insights into biohydrogen production by microalgae – from biophotolysis to dark fermentation. Bioresour Technol 2017;227:373–87. https://doi.org/10.1016/j.biortech.2016.12.104.

[5] Khosravitabar F, Hippler M. A new approach for improving microalgal biohydrogen photoproduction based on safe & fast oxygen consumption. Int J Hydrogen Energy 2019;44:17835–44. https://doi.org/10.1016/j.ijhydene.2019.05.038.

[6] Elshobary ME, Zabed HM, Yun J, Zhang G, Qi X. Recent insights into microalgae-assisted microbial fuel cells for generating sustainable bioelectricity. Int J Hydrogen Energy 2021;46:3135–59. https://doi.org/10.1016/j.ijhydene.2020.06.251.

[7] Jaiswal KK, Kumar V, Vlaskin MS, Sharma N, Rautela I, Nanda M, et al. Microalgae fuel cell for wastewater treatment: recent advances and challenges. J Water Process Eng 2020;38:101549. https://doi.org/10.1016/j.jwpe.2020.101549.

[8] Eroglu E, Melis A. Microalgal hydrogen production research. Int J Hydrogen Energy 2016;41:12772–98. https://doi.org/10.1016/j.ijhydene.2016.05.115.

[9] Lakatos GE, Ranglová K, Manoel JC, Grivalský T, Kopecký J, Masojídek J. Bioethanol production from microalgae polysaccharides. Folia Microbiol 2019;64:627–44. https://doi.org/10.1007/s12223-019-00732-0.

[10] Chen C-Y, Chang H-Y, Chang J-S. Producing carbohydrate-rich microalgal biomass grown under mixotrophic conditions as feedstock for biohydrogen production. Int J Hydrogen Energy 2016;41:4413–20. https://doi.org/10.1016/j.ijhydene.2015.05.163.

[11] Costa JAV, Freitas BCB, Rosa GM, Moraes L, Morais MG, Mitchell BG. Operational and economic aspects of Spirulina-based biorefinery. Bioresour Technol 2019;292:121946. https://doi.org/10.1016/j.biortech.2019.121946.

[12] Sahrin NT, Shiong Khoo K, Wei Lim J, Shamsuddin R, Musa Ardo F, Rawindran H, et al. Current perspectives, future challenges and key technologies of biohydrogen production for building a carbon–neutral future: a review. Bioresour Technol 2022;364:128088. https://doi.org/10.1016/j.biortech.2022.128088.

[13] Zheng Y, Li Y, Zhang Y, Zhang R, Zhang Q, Zhang Y, et al. Fractionation, physicochemical properties, nutritional value, antioxidant activity and ACE inhibition of palm kernel expeller protein. RSC Adv 2015;5:12613–23. https://doi.org/10.1039/C4RA13352H.

[14] Sabeeh M, Zeshan, Liaquat R, Maryam A. Effect of alkaline and alkaline-photocatalytic pretreatment on characteristics and biogas production of rice straw. Bioresour Technol 2020;309:123449. https://doi.org/10.1016/j.biortech.2020.123449.

[15] Mankar AR, Pandey A, Modak A, Pant KK. Pretreatment of lignocellulosic biomass: a review on recent advances. Bioresour Technol 2021;334:125235. https://doi.org/10.1016/j.biortech.2021.125235.

[16] Li S-H, Liu S, Colmenares JC, Xu Y-J. A sustainable approach for lignin valorization by heterogeneous photocatalysis. Green Chem 2016;18:594–607. https://doi.org/10.1039/C5GC02109J.

[17] Liu X, Duan X, Wei W, Wang S, Ni B-J. Photocatalytic conversion of lignocellulosic biomass to valuable products. Green Chem 2019;21:4266–89. https://doi.org/10.1039/C9GC01728C.

[18] Xiang Z, Han W, Deng J, Zhu W, Zhang Y, Wang H. Photocatalytic conversion of lignin into chemicals and fuels. ChemSusChem 2020;13:4199–213. https://doi.org/10.1002/cssc.202000601.

[19] Nath RK, Zain MFM, Jamil M. An environment-friendly solution for indoor air purification by using renewable photocatalysts in concrete: a review. Renew Sustain Energy Rev 2016;62:1184–94. https://doi.org/10.1016/j.rser.2016.05.018.

[20] Sahrin NT, Nawaz R, Fai Kait C, Lee SL, Wirzal MDH. Visible light photodegradation of formaldehyde over TiO2 nanotubes synthesized via electrochemical anodization of titanium foil. Nanomaterials 2020;10. https://doi.org/10.3390/nano10010128.

[21] Hyam RS, Choi D. Effects of titanium foil thickness on TiO2 nanostructures synthesized by anodization. RSC Adv 2013;3:7057–63. https://doi.org/10.1039/C3RA40581H.

[22] Liang H, Li X. Effects of structure of anodic TiO2 nanotube arrays on photocatalytic activity for the degradation of 2,3-dichlorophenol in aqueous solution. J Hazard Mater 2009;162:1415–22. https://doi.org/10.1016/j.jhazmat.2008.06.033.

[23] Nomanbhay SM, Hussain R, Palanisamy K. Microwave-assisted alkaline pretreatment and microwave assisted enzymatic saccharification of oil palm empty fruit bunch fiber for enhanced fermentable sugar yield 2013. 2013. https://doi.org/10.4236/jsbs.2013.31002.

[24] Shamsuri A, Daik R, Zainudin E, Tahir P. Compatibilization of HDPE/agar biocomposites with eutectic-based ionic liquid containing surfactant. J Reinforc Plast Compos 2014;33:440–53. https://doi.org/10.1177/0731684413516688.

[25] Chen Y, Yin Y, Wang J. Biohydrogen production using macroalgal biomass of Laminaria japonica pretreated by gamma irradiation as substrate. Fuel 2022;309:122179. https://doi.org/10.1016/j.fuel.2021.122179.

[26] Maryam A, Zeshan, Badshah M, Sabeeh M, Khan SJ. Enhancing methane production from dewatered waste activated sludge through alkaline and

photocatalytic pretreatment. Bioresour Technol 2021;325:124677. https://doi.org/10.1016/j.biortech.2021.124677.
[27] Qiao W, Yan X, Ye J, Sun Y, Wang W, Zhang Z. Evaluation of biogas production from different biomass wastes with/without hydrothermal pretreatment. Renew Energy 2011;36:3313–8. https://doi.org/10.1016/j.renene.2011.05.002.
[28] Alvarado-Morales M, Tsapekos P, Awais M, Gulfraz M, Angelidaki I. TiO2/UV based photocatalytic pretreatment of wheat straw for biogas production. Anaerobe 2017;46:155–61. https://doi.org/10.1016/j.anaerobe.2016.11.002.
[29] Corro G, Pal U, Cebada S. Enhanced biogas production from coffee pulp through delignocellulosic photocatalytic pretreatment. Energy Sci Eng 2014;2:177–87. https://doi.org/10.1002/ese3.44.
[30] Tedesco S, Hurst G, Imtiaz A, Ratova M, Tosheva L, Kelly P. TiO2 supported natural zeolites as biogas enhancers through photocatalytic pre-treatment of Miscanthus x giganteous crops. Energy 2020;205:117954. https://doi.org/10.1016/j.energy.2020.117954.
[31] Mahdavi M, Mirmohammadi M, Baghdadi M, Mahpishanian S. Visible light photocatalytic degradation and pretreatment of lignin using magnetic graphitic carbon nitride for enhancing methane production in anaerobic digestion. Fuel 2022;318:123600. https://doi.org/10.1016/j.fuel.2022.123600.
[32] Machado AEH, Furuyama AM, Falone SZ, Ruggiero R, Perez D da S, Castellan A. Photocatalytic degradation of lignin and lignin models, using titanium dioxide: the role of the hydroxyl radical. Chemosphere 2000;40:115–24. https://doi.org/10.1016/S0045-6535(99)00269-6.
[33] Lekelefac CA, Czermak P. Degradation of lignin derivatives by photocatalysts. IntechOpen; 2016. https://doi.org/10.5772/62585.
[34] Yu J, Wang B. Effect of calcination temperature on morphology and photoelectrochemical properties of anodized titanium dioxide nanotube arrays. Appl Catal B Environ 2010;94:295–302. https://doi.org/10.1016/j.apcatb.2009.12.003.
[35] Li HF, Qiu KJ, Yuan W, Zhou FY, Wang BL, Li L, et al. Screening on binary Ti alloy with excellent mechanical property and castability for dental prosthesis application. Sci Rep 2016;6:37428. https://doi.org/10.1038/srep37428.
[36] Liu R, Yang W-D, Qiang L-S, Wu J-F. Fabrication of TiO2 nanotube arrays by electrochemical anodization in an NH4F/H3PO4 electrolyte. Thin Solid Films 2011;519:6459–66. https://doi.org/10.1016/j.tsf.2011.04.231.
[37] Erol M, Dikici T, Toparli M, Celik E. The effect of anodization parameters on the formation of nanoporous TiO2 layers and their photocatalytic activities. J Alloys Compd 2014;604:66–72. https://doi.org/10.1016/j.jallcom.2014.03.105.
[38] Granada-Ramirez DA, Cardona-Bedoya JA, Hernandez-Rojas U, Pulzara-Mora A, Delgado-Rosero MI, Durán-Ledezma AA, et al. Assessment of Cr doping on TiO2 thin films deposited by a wet chemical method. Ceram Int 2023;49:30347–54. https://doi.org/10.1016/j.ceramint.2023.06.293.
[39] Zhang W, Liu Y, Guo F, Liu J, Yang F. Kinetic analysis of the anodic growth of TiO2 nanotubes: effects of voltage and temperature. J Mater Chem C 2019;7:14098–108. https://doi.org/10.1039/C9TC04532E.
[40] Omidvar H, Goodarzi S, Seif A, Azadmehr AR. Influence of anodization parameters on the morphology of TiO2 nanotube arrays. Superlattice Microst 2011;50:26–39. https://doi.org/10.1016/j.spmi.2011.04.006.
[41] Lai CW, Sreekantan S. Effect of applied potential on the formation of self-organized nanotube arrays and its photoelectrochemical response. J Nanomater 2011;2011:e142463. https://doi.org/10.1155/2011/142463.
[42] Kapusta-Kołodziej J, Syrek K, Pawlik A, Jarosz M, Tynkevych O, Sulka GD. Effects of anodizing potential and temperature on the growth of anodic TiO2 and its photoelectrochemical properties. Appl Surf Sci 2017;396:1119–29. https://doi.org/10.1016/j.apsusc.2016.11.097.
[43] Qin L, Chen Q, Lan R, Jiang R, Quan X, Xu B, et al. Effect of anodization parameters on morphology and photocatalysis properties of TiO2 nanotube arrays. J Mater Sci Technol 2015;31:1059–64. https://doi.org/10.1016/j.jmst.2015.07.012.
[44] Gong D, Grimes CA, Varghese OK, Hu W, Singh RS, Chen Z, et al. Titanium oxide nanotube arrays prepared by anodic oxidation. J Mater Res 2001;16:3331–4. https://doi.org/10.1557/JMR.2001.0457.
[45] Nawaz R, Kait CF, Chia HY, Isa MH, Huei LW, Sahrin NT, et al. Manipulation of the Ti3+/Ti4+ ratio in colored titanium dioxide and its role in photocatalytic degradation of environmental pollutants. Surface Interfac 2022;32:102146. https://doi.org/10.1016/j.surfin.2022.102146.
[46] Singh J, Sahu K, Singh R, Som T, Kotnala RK, Mohapatra S. Thermal annealing induced strong photoluminescence enhancement in Ag-TiO2 plasmonic nanocomposite thin films. J Alloys Compd 2019;786:750–7. https://doi.org/10.1016/j.jallcom.2019.01.322.
[47] Hurum DC, Agrios AG, Gray KA, Rajh T, Thurnauer MC. Explaining the enhanced photocatalytic activity of degussa P25 mixed-phase TiO2 using EPR. J Phys Chem B 2003;107:4545–9. https://doi.org/10.1021/jp0273934.
[48] Sorathiya K, Mishra B, Kalarikkal A, Reddy KP, Gopinath CS, Khushalani D. Enhancement in rate of photocatalysis upon catalyst recycling. Sci Rep 2016;6:35075. https://doi.org/10.1038/srep35075.
[49] Altomare M, Pozzi M, Allieta M, Bettini LG, Selli E. H2 and O2 photocatalytic production on TiO2 nanotube arrays: effect of the anodization time on structural features and photoactivity. Appl Catal B Environ 2013;136–137:81–8. https://doi.org/10.1016/j.apcatb.2013.01.054.
[50] Xiao P, Liu D, Garcia BB, Sepehri S, Zhang Y, Cao G. Electrochemical and photoelectrical properties of titania nanotube arrays annealed in different gases. Sensor Actuator B Chem 2008;134:367–72. https://doi.org/10.1016/j.snb.2008.05.005.
[51] Weon S, Choi E, Kim H, Kim JY, Park H-J, Kim S, et al. Active {001} facet exposed TiO2 nanotubes photocatalyst filter for volatile organic compounds removal: from material development to commercial indoor air cleaner application. Environ Sci Technol 2018;52:9330–40. https://doi.org/10.1021/acs.est.8b02282.
[52] Wint THM, Smith MF, Chanlek N, Chen F, Oo TZ, Songsiriritthigul P. Physical origin of diminishing photocatalytic efficiency for recycled TiO2 nanotubes and Ag-loaded TiO2 nanotubes in organic aqueous solution. Catalysts 2020;10:737. https://doi.org/10.3390/catal10070737.